

Article

# Electroforming as a Novel One-Step Manufacturing Method of Structured Aluminum Foil Current Collectors for Lithium-Ion Batteries

**Phillip Scherzl** , **Michael Kaupp**, **Wassima El Mofid** and **Timo Sörgel** \*

Center for Electrochemical Surface Technology ZEO, Aalen University of Applied Sciences, Beethovenstr. 1, 73430 Aalen, Germany

\* Correspondence: timo.soergel@hs-aalen.de

**Abstract:** Conventionally, cathode current collectors for lithium-ion batteries (LIB) consist of an aluminum foil generally manufactured by a rolling process. In the present work, a novel one-step manufacturing method of structured aluminum foil current collectors for lithium-ion batteries by electroforming is introduced. For this, a low-temperature chloride-based ionic liquid was used as an electrolyte and a rotating cylinder out of stainless steel as a temporary substrate. It was shown that the structure of the aluminum foils can be adjusted from dense and flat to three-dimensional by choosing an appropriate substrate rotation speed and current density. Scanning electron microscopy (SEM) and white light interferometry (WLI) were utilized to analyze the foils' surface morphology, structure and topography. The SEM analysis of the aluminum foils showed that the rolling process produced a foil with small grains, while electrodeposition resulted in foils with different degrees of grain growth and seed formation. This was in total agreement with WLI results that revealed significant differences in terms of roughness parameters, including the peak-to-valley difference  $R_{pv}$ , the root-mean-square roughness  $R_q$  and the arithmetic mean roughness  $R_a$ . These were, respectively, equal to 6.8  $\mu\text{m}$ , 0.35  $\mu\text{m}$  and 0.279  $\mu\text{m}$  for the state-of-the-art foil and up to 96.6  $\mu\text{m}$ , 10.92  $\mu\text{m}$  and 8.783  $\mu\text{m}$  for the structured electroformed foil. Additionally, cyclic voltammetry (CV) of the aluminum foils was used to investigate their passivation behavior within the typical LIB cathode potential operation window. The strong decrease in the current density during the second cycle compared to the first cycle, where an anodic peak appeared between 4.0 and 4.4 V vs. Li/Li<sup>+</sup>, demonstrated that passivation occurs in the same manner as observed for commercial Al current collectors.



**Citation:** Scherzl, P.; Kaupp, M.; El Mofid, W.; Sörgel, T. Electroforming as a Novel One-Step Manufacturing Method of Structured Aluminum Foil Current Collectors for Lithium-Ion Batteries. *Batteries* **2023**, *9*, 422. <https://doi.org/10.3390/batteries9080422>

Academic Editors: Carlos Ziebert and Matthieu Dubarry

Received: 16 June 2023

Revised: 19 July 2023

Accepted: 9 August 2023

Published: 12 August 2023



**Copyright:** © 2023 by the authors. Licensee MDPI, Basel, Switzerland. This article is an open access article distributed under the terms and conditions of the Creative Commons Attribution (CC BY) license (<https://creativecommons.org/licenses/by/4.0/>).

## 1. Introduction

Numerous efforts are constantly underway to replace fossil fuels with renewable energy systems, with the aim of reducing the greenhouse gas emissions associated with power generation. Nevertheless, the unevenness of renewable energy generation and the timing mismatch between supply and demand limit their large-scale integration, especially when renewables are the primary energy source. One way to meet this challenge is through the use of electrical energy storage systems (ESSs) [1–3]. Among the various storage technologies, battery storage systems are widely used, more particularly lithium-ion batteries (LIBs), which represent the majority of battery storage systems currently deployed [4,5]. These are also playing a crucial role in the electrification of the transport sector, especially for electric cars, helping likewise to reduce greenhouse gas emissions. Additionally, their excellent performance in terms of high gravimetric and volumetric energy as well as power densities, compared to other commonly used battery technologies, makes them the preferred choice in other fields such as consumer electronics [6–8]. A

conventional LIB consists of three main components: an anode, a cathode and an electrolyte-soaked separator. The electrolyte generally used is a mixture of ethylene carbonate (EC) with dimethyl carbonate (DMC) or diethyl carbonate (DEC) or ethyl methyl carbonate (EMC), plus lithium hexafluorophosphate ( $\text{LiPF}_6$ ), which acts as a conductive salt. The anode, meanwhile, is mainly made of graphite as an electrochemically active  $\text{Li}^+$  host mostly mixed with styrene butadiene rubber (SBR) as a binder. These components are then coated on a copper foil, which represents the current collector. For the cathode side, an aluminum foil is coated with a mixture of active material (e.g.,  $\text{LiNi}_x\text{Mn}_y\text{Co}_z\text{O}_2$  (NMC),  $\text{LiFePO}_4$  (LFP) or  $\text{LiNi}_{0.8}\text{Co}_{0.15}\text{Al}_{0.05}\text{O}_2$  (NCA)), a polymeric binder such as polyvinylidene fluoride (PVDF) and a conductive agent such as carbon black (CB) [9–12].

The functioning of an LIB is based on several key elements. While the active materials in the electrodes are storing the  $\text{Li}^+$  ions, the electrolyte is responsible for transporting them between the two electrodes. Meanwhile, current collectors play a crucial role by collecting the electrons released or consumed during electrochemical reactions at the electrodes and transporting them through the external circuit [13,14]. According to studies carried out by He et al., aluminum foil current collectors account for 6.9 wt% of the total weight of an LIB cell while the copper foil accounts for 8.1 wt% [15]. The latter can be produced either by rolling [16] or by electrodeposition [17,18]. Nowadays, thicknesses can be as low as 10  $\mu\text{m}$  for high-energy density cells [19]. In this respect, electroforming is especially suitable for the manufacturing of current collectors with thicknesses well below 10  $\mu\text{m}$ . Up to now, apart from copper [20], only nickel foils are commercially produced by electroforming process. The latter is also used for the production of Ni foams [21]. The feature of structured current collector foils is again reported mainly for copper foils [22–25]. Yet for cathodes, nickel foams are being used on a large scale in commercial “nickel” ( $\text{NiO(OH)}/\text{Ni(OH)}_2$ ) cathodes, nowadays mainly for nickel metal hydride batteries. Furthermore, the concept of foam-type cathodes is also exploited for the cathode side, either in form of nickel [26] or aluminum foams [27]. Additionally, hybrid forms of structured nickel/aluminum current collectors are being used [28]. On the cathode side, state-of-the-art unstructured aluminum current collectors show thicknesses in the range between 10 and around 25  $\mu\text{m}$  [16] and can usually be thinned by a rolling process to the desired thickness [19].

Up to now, electroforming, as in the case of copper foils, has not yet been used as a manufacturing process for aluminum current collectors. Publications on the electroforming of aluminum foils are extremely limited. This can be explained by the fact that aluminum deposition from aqueous electrolytes is not possible due to the negative half-cell potential of  $\text{Al}/\text{Al}^{3+}$  (−1.66 V vs. SHE) [29]. Nevertheless, some studies have been carried out in this field. For example, Tu et al. [30] reported the electroforming of aluminum foils on a 10 mm diameter graphite disc electrode from low-temperature ionic liquid  $\text{AlCl}_3$ —1-Butyl-3-methyl-imidazolium chloride (2:1 molar ratio) using a three-electrode system. Further works have also been carried out by Ui et al. [31–36] regarding the electroforming of aluminum foils with smooth surface by pulse deposition and/or addition of 1,10-phenanthroline anhydrate to the  $\text{AlCl}_3$ —1-Ethyl-3-methyl-imidazolium chloride ([EMIIm]Cl) (2:1 molar ratio) electrolyte. In their experiments, a titanium plate with an area of 0.95  $\text{cm}^2$  is used as cathode. Ruan et al. reported that they achieved free-standing Al–Mn alloy foils by dissolving the copper substrate in nitric acid after electrodeposition in  $\text{AlCl}_3$ —1-Ethyl-3-methyl-imidazolium chloride (2:1 molar ratio) electrolyte with the addition of  $\text{MnCl}_2$  [37].

In the current study, stainless steel (SAE 304) cylinders are electroplated with aluminum from the ionic liquid  $\text{AlCl}_3$ —[EMIIm]Cl in a molar ratio of 1.5:1. Various rotation speeds of the cylinders and current densities are applied during the electroforming process. The resulting deposits are then peeled off from the substrates to form separate aluminum foils. These are then analyzed and characterized to assess their properties. Cyclic voltammetry (CV) is carried out to study the electrochemical behavior of aluminum foils in an electrolyte for lithium-ion batteries. Imaging techniques such as scanning electron microscopy (SEM) and white light interferometry (WLI) are used to visualize and analyze the

morphology and topography of the resulting aluminum foils. Such detailed investigations yield valuable information on the deposition quality and the structural properties of aluminum foils produced by electroforming. They also provide important data for assessing the suitability of such aluminum foils as current collectors for lithium-ion batteries.

## 2. Materials and Methods

### 2.1. Materials and Chemicals

The electrolyte for aluminum deposition was prepared from [EMIm]Cl (>98%, IoLiTec Ionic Liquids Technologies GmbH, Heilbronn, Germany) and AlCl<sub>3</sub> (granules, 99%, abcr GmbH, Karlsruhe, Germany). Additionally, an aluminum wire with 1.0 mm diameter ( $\geq 99.999\%$ , Fisher Scientific GmbH, Schwerte, Germany) as a reference electrode, two aluminum sheets of 2.0 mm thickness (192  $\times$  30 mm, 99.99%, abcr GmbH, Karlsruhe, Germany) as anodes and a stainless steel (SAE 304) cylinder (Hans-Erich Gemmel & Co. GmbH, Berlin, Germany) with an outer diameter of 25 mm as substrate were acquired. Dichloromethane (99.8+%, Acros Organics, Geel, Belgium) was dried with 4 Å pore size molecular sieves (Carl Roth GmbH + Co. KG, Karlsruhe, Germany) prior to its use for rinsing purpose.

### 2.2. Preparation of the Electrolyte and Electrodes

To remove residual water of the [EMIm]Cl, the latter was placed in two round-bottom flasks and dried at a temperature of 60 °C and a pressure below 10 mbar for a duration of 52 h using a Schlenk line. The water content of the salt was measured by Karl-Fischer titration (831 KF Coulometer + 774 Oven Sample Processor, Deutsche METROHM GmbH & Co. KG, Filderstadt, Germany). All subsequent work was carried out in a nitrogen-filled glovebox (MBraun, Garching, Germany) with H<sub>2</sub>O and O<sub>2</sub> contents below 0.5 ppm. AlCl<sub>3</sub> was mixed with [EMIm]Cl in a glass bottle in small portions and under continuous magnetic stirring at 185 rpm, due to the exothermic aspect of the reaction, until the mixture became fully liquid. Afterwards, the electrolyte was further stirred during 24 h for better homogenization. Thereafter, an aluminum foil was placed inside the solution for a further 72 h to purify it from more noble metal impurities by the process of cementation. After filtration, a clear and slightly yellowish liquid was obtained.

Concerning the electrodes preparation, an aluminum wire was fixed in a thin glass tube with acrylic glue (Acryfix® 1R 0192, Evonik AG, Essen, Germany) in a way that 10 mm still protruded. The stainless-steel cylinder was subsequently cut into smaller ones with 40 mm length which were sanded with emery paper (180, 320, 800, 1200, 2500) to achieve a shiny surface with no visible defects. The surface roughness of the cylinder was determined with a white light interferometer (Zegage Profiler with ZeMaps v.1.11, Zemetrics, Inc., Tucso, AZ, USA). The edges of the cylinders, as well as a longitudinal strip, were covered with PTFE adhesive tape (PLOFLON® PTFE Klebefilm, W + B Datentechnik GmbH, Hagen, Germany). The remaining surface area was 210 mm<sup>2</sup> (30  $\times$  70 mm).

### 2.3. Microstructural and Electrochemical Characterization

The morphological investigation of the aluminum foils was carried out by SEM (Gemini LEO 1525, ZEISS AG, Oberkochen, Germany) and WLI. Each WLI measurement was repeated three times and the results were averaged. Moreover, further information about the microstructure was achieved through the examination of the foils' cross sections using a light microscope (digital light microscope VHX 6000, KEYENCE DEUTSCHLAND GmbH, Neu-Isenburg, Germany).

Pieces of 12 mm diameter were stamped out of the aluminum foils and dried at 60 °C with a pressure below 10 mbar, overnight. For electrochemical characterization, a three-electrode cell (TSC Battery, rhd instruments GmbH & Co. KG, Darmstadt, Germany) was used. Two discs of 12 mm diameter out of aluminum foil and lithium (99.9%, Sigma-Aldrich Chemie GmbH, Taufkirchen, Germany), with a thickness of 0.75 mm, stand for the working and counter electrodes, respectively. A small lithium tip of approximately 1.2-mm-thickness served as a reference electrode. Three 25-μm-thick separators (12 mm diameter,

Celgard 2500, Celgard LLC, Charlotte, NC, USA) were placed between the counter and the working electrodes. The electrolyte consisted of 50  $\mu$ L of 1 M LiPF<sub>6</sub> in EC/DEC (1:1 by volume, Sigma-Aldrich Chemie GmbH, Taufkirchen, Germany). The cells' assembly was carried out in an argon-filled glovebox ( $c(H_2O) < 0.1$  ppm,  $c(O_2) < 0.1$  ppm, MBraun, Garching, Germany). After a resting period of 12 h, CVs were recorded between 2.7 and 5.0 V vs. Li/Li<sup>+</sup> with a scan rate of 10 mV/s. The starting point was the open circuit voltage OCV and the potential was ramped to the lower vertex potential first.

For comparison, all techniques were likewise applied to a state-of-the-art laboratory aluminum current collector foil (20  $\mu$ m thickness, EN AW 8079, KORFF AG, Oberbipp, Switzerland) taken as reference.

### 3. Results

#### 3.1. Electroforming of Aluminum Foils

The deposition experiments were carried out using a three-electrode system and 1000 mL of the electrolyte in a 2000 mL beaker. Two aluminum sheets served as counter electrodes, a cylinder as working electrode and the aluminum wire as reference electrode. All electrodes were initially cleaned with isopropyl alcohol. Counter electrodes were fixed in parallel at a distance of 95 mm. The cylinder was placed equally distant between the counter electrodes. During deposition experiments the cylinder was rotating horizontally, as shown in Figure 1a.

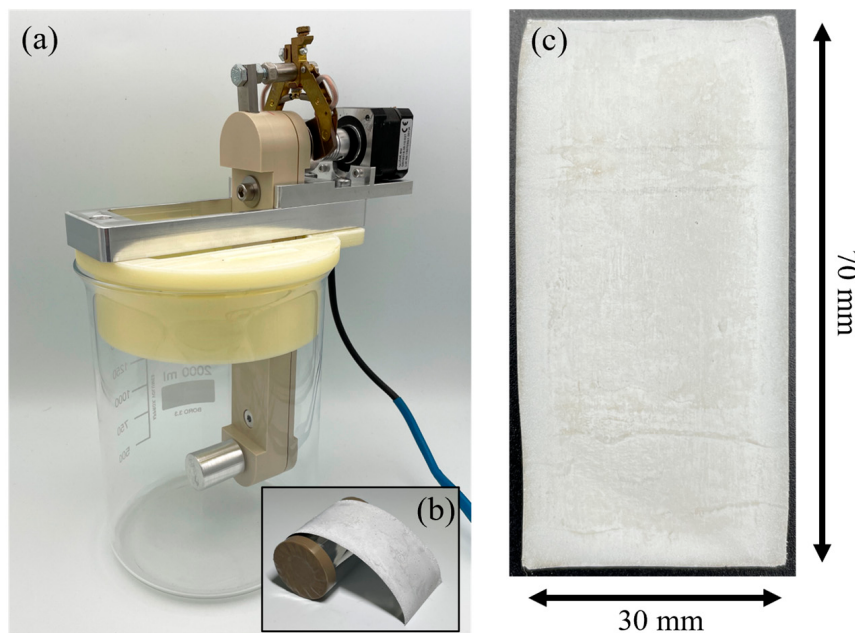


**Figure 1.** (a) Experimental setup for electroforming with a rotating cylinder as a substrate. (b) Electroformed aluminum foil during detachment from the masked cylinder. (c) Top-view photograph of an aluminum foil electroformed at a rotation speed of 20 rpm and a current density of 15 mA/cm<sup>2</sup>.

To study the effects of different rotation speeds of the cylinder as well as the current density on the aluminum foil properties, these two parameters were varied. The electrolyte temperature and the stirring velocity of the electrolyte, with a 40 mm magnetic stirring bar, were kept constant at 50 °C and approx. 250 rpm, respectively. A potentiostat (VSP with booster VMP3B-20 20 A/20 V, Biologic Science Instruments GmbH, Seyssinet-Pariset, France) was used for applying currents and measuring the electrode potentials during deposition accordingly. The target thickness of the aluminum layers was 20  $\mu$ m assuming 100% current efficiency. Table 1 shows the applied deposition parameters.

**Table 1.** Parameters for aluminum deposition to achieve a 20  $\mu\text{m}$  layer thickness by assuming 100% current efficiency.

Substrate Rotation Speed [rpm]	Current Density [ $\text{mA}/\text{cm}^2$ ]
20	15
20	10
20	5
10	15
10	10
10	5
1	15
1	10
1	5
1	20

After deposition, the substrate rotating with a speed of 30 rpm was rinsed three times for 1 min in dichloromethane. Then, it was taken out of the glovebox. The PTFE-tape was removed and the substrate was rinsed again with deionized water and isopropyl alcohol. Finally, the aluminum layer could be peeled off with the help of a scalpel.

Figure 1b,c show an example of an electroformed aluminum foil during and after detachment from the cylinder. For the deposition of the aluminum foil in Figure 1c a cylinder rotation speed of 20 rpm and a current density of 15  $\text{mA}/\text{cm}^2$  were used.

### 3.2. Microstructural Characterization

In order to investigate the correlation between deposition parameters and the microstructure of the electroformed aluminum foils, a detailed characterization was conducted using a variety of techniques. The aluminum foils were characterized by digital light microscopy, in particular cross-sectional analysis, as well as SEM and WLI for top view observations. Figure 2 displays cross sectional images of (a) a state-of-the-art laboratory aluminum current collector foil and (b) to (d) electroformed aluminum foils deposited using different parameter sets. More specifically, (b) corresponds to a deposition process carried out at a rotational speed of 1 rpm and a current density of 20  $\text{mA}/\text{cm}^2$ , (c) represents deposition at 1 rpm and 10  $\text{mA}/\text{cm}^2$  and (d) illustrates deposition at 20 rpm and 10  $\text{mA}/\text{cm}^2$ . The images were captured at two magnifications 200 $\times$  (lower) and 800 $\times$  (upper).

Image (a) reveals that the state-of-the-art foil has a dense structure with smooth top and bottom surfaces. In comparison, the electroformed foils in images (b) to (d) only have a smooth bottom side which is related to the very low surface roughness of the substrate on which the foils have been deposited and whose negative geometry is reproduced during electroforming. Since the bottom side of the film replicates the substrate surface, its roughness is essentially determined by that of the substrate surface which was also measured on three different profile lines on three substrates by WLI. Therefore, various roughness parameters were measured, including the peak-to-valley difference  $R_{\text{pv}}$ , the root-mean-square roughness  $R_q$  and the arithmetic mean roughness  $R_a$ . Hence, the results obtained for the substrate surface roughness are  $R_{\text{pv}} = 0.5 \pm 0.2 \mu\text{m}$ ,  $R_q = 0.04 \pm 0.02 \mu\text{m}$  and  $R_a = 0.032 \pm 0.003 \mu\text{m}$ ). Consequently, the smoothness observed on the underside of electroformed foils can be attributed to the exceptionally low roughness of the substrate surface, as confirmed by its measured values of  $R_{\text{pv}}$ ,  $R_q$  and  $R_a$ . This allows to also influence and specify the bottom-side surface characteristics. The roughness of the top side, on the other hand, reveals significant differences from that of the state-of-the-art foil. In particular, the foils in images (c) and (d) show the presence of pores in the electroformed foils. It is obvious that the roughness strongly depends on the deposition parameters of the aluminum layer. By comparing images (b) and (c), it can be seen that, at constant rotation speed of the cylinder substrate, a higher current density leads to a less structured surface. Additionally, the rotation speed of the substrate cylinder also influences the roughness. The foil in image (c) was produced at lower rotation speed than the foil in image (d) and, thus, appears to

be more compact and homogenous. Also, image (d) reveals a greater portion of pores compared to image (c).

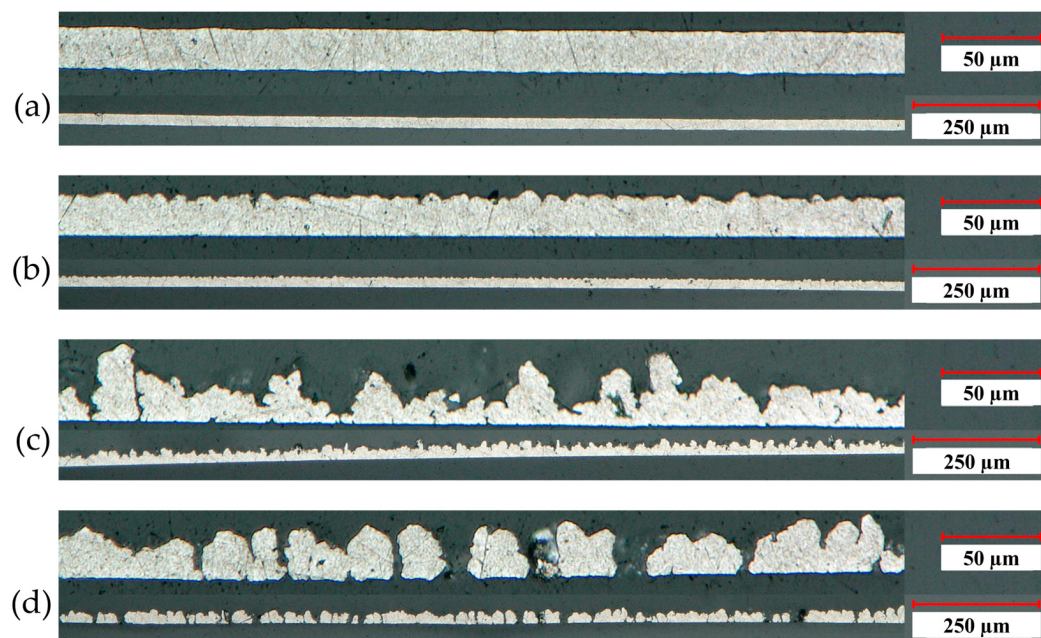


**Figure 2.** Cross sections with magnifications of 200 $\times$  (lower image) and 800 $\times$  (upper image) of (a) a state-of-the-art laboratory aluminum current collector foil and (b–d) electroformed aluminum foils deposited with (b) 1 rpm and 20 mA/cm $^2$ , (c) 1 rpm and 10 mA/cm $^2$  and (d) 20 rpm and 10 mA/cm $^2$ .

The aluminum foils' surfaces shown in Figure 2 were further examined by WLI to obtain detailed information on the surface topography. The resulting images are displayed in Figure 3. The naming (a–d) of the single images was conducted in analogy to Figure 2. At mid-height on each image, a horizontal line was drawn, indicating the position of the measured profile lines as presented in Figure 4. The roughness values corresponding to these profile lines are also provided.

Analysis of the WLI images in Figure 3, together with the corresponding values for areal roughness provided in Table 2, delivers further information on the surface characteristics of the aluminum foils. Observing the coloring of the images, which provides a qualitative assessment of the surface roughness variations, one can easily see that the roughness increases from image (a) to image (d). Together with the measured profile lines in Figure 4, this observation is consistent with the results obtained from the cross-sectional analysis in Figure 2.

**Table 2.** Areal roughness values of white light interferometer images shown in Figure 3. Images (a–d) belong to (a) a state-of-the-art laboratory aluminum current collector foil and (b–d) electroformed aluminum foils deposited with (b) 1 rpm and 20 mA/cm $^2$ , (c) 1 rpm and 10 mA/cm $^2$  and (d) 20 rpm and 10 mA/cm $^2$ .

Image	S <sub>pv</sub> [μm]	S <sub>q</sub> [μm]	S <sub>a</sub> [μm]
(a)	6.8	0.35	0.279
(b)	29.1	1.38	0.984
(c)	58.9	7.55	6.014
(d)	96.6	10.92	8.783

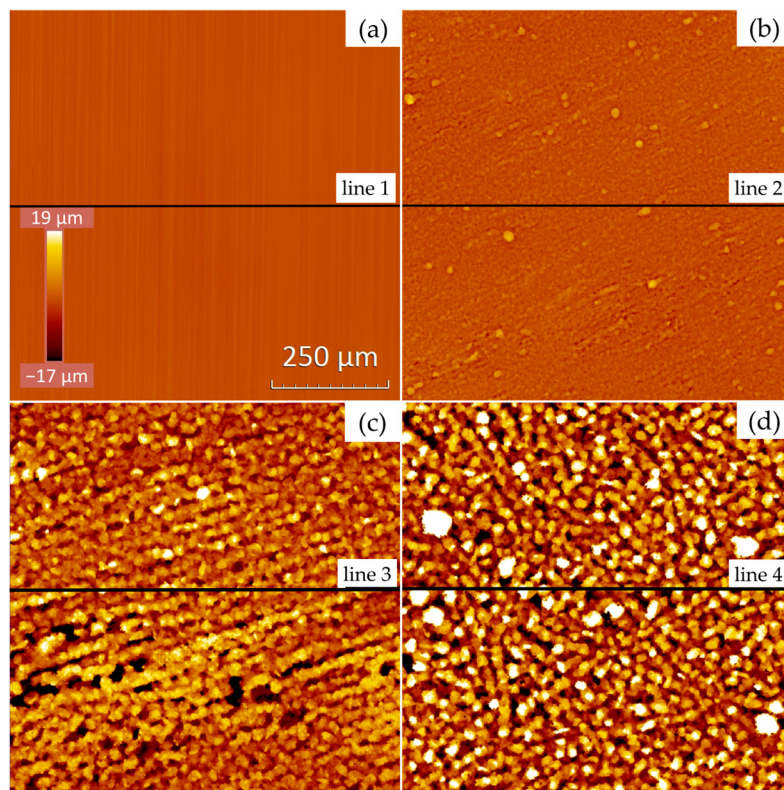


**Figure 3.** WLI images of (a) a state-of-the-art laboratory aluminum current collector foil and (b–d) electroformed aluminum foils deposited with (b) 1 rpm and  $20 \text{ mA}/\text{cm}^2$ , (c) 1 rpm and  $10 \text{ mA}/\text{cm}^2$  and (d) 20 rpm and  $10 \text{ mA}/\text{cm}^2$ . Lines 1–4 (—) show the position of the measured profile lines from Figure 4.

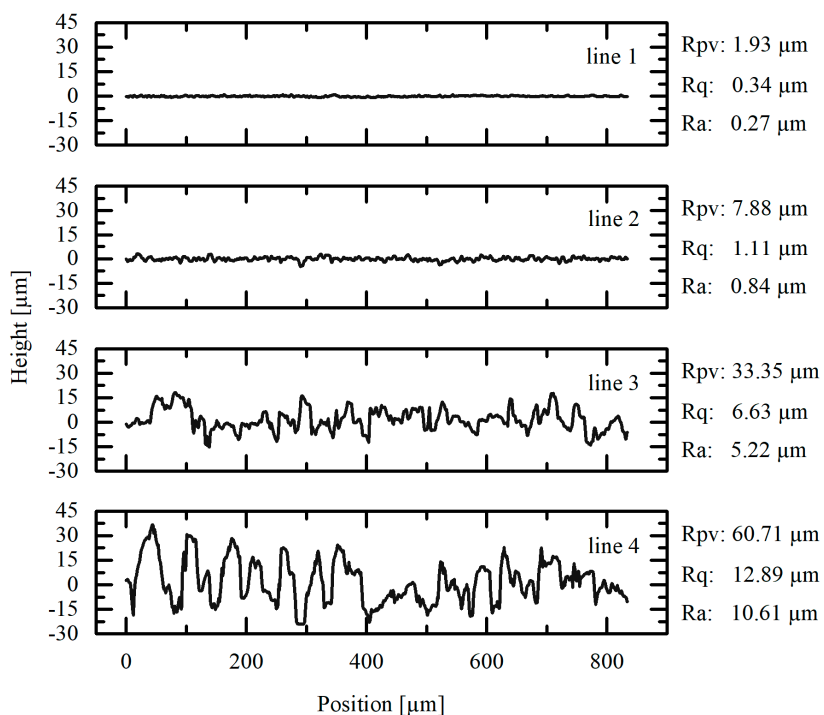


**Figure 4.** Measured profile lines from white light interferometer images shown in Figure 3. Lines 1–4 belong to (1) a state-of-the-art laboratory aluminum current collector foil and (2–4) electroformed aluminum foils deposited with (2) 1 rpm and  $20 \text{ mA}/\text{cm}^2$ , (3) 1 rpm and  $10 \text{ mA}/\text{cm}^2$  and (4) 20 rpm and  $10 \text{ mA}/\text{cm}^2$ .

Figure 5 shows SEM images of the different aluminum foils. The naming of the images (a) to (d) was conducted in accordance with the corresponding Figures 2 and 3. Image (a) shows a typical surface of a foil obtained by a rolling process. As can be seen, the grain size of the electrodeposited aluminum increases from image (b) to (d). In image (b) the grains have a predominantly fine structure, with occasional larger, coarser grains scattered across the surface. This variation in grain size is indicative of the applied electroplating process. In contrast, image (d) shows a distinct grain morphology characterized by the presence of very large grains. This suggests that the deposition parameters used to produce the aluminum foil in image (d) have resulted in more pronounced grain growth vs. seed formation. Image (c) presents an intermediate state between images (b) and (d). It comprises a combination of fine and coarse grains, indicating a mixed-grain structure on the surface.

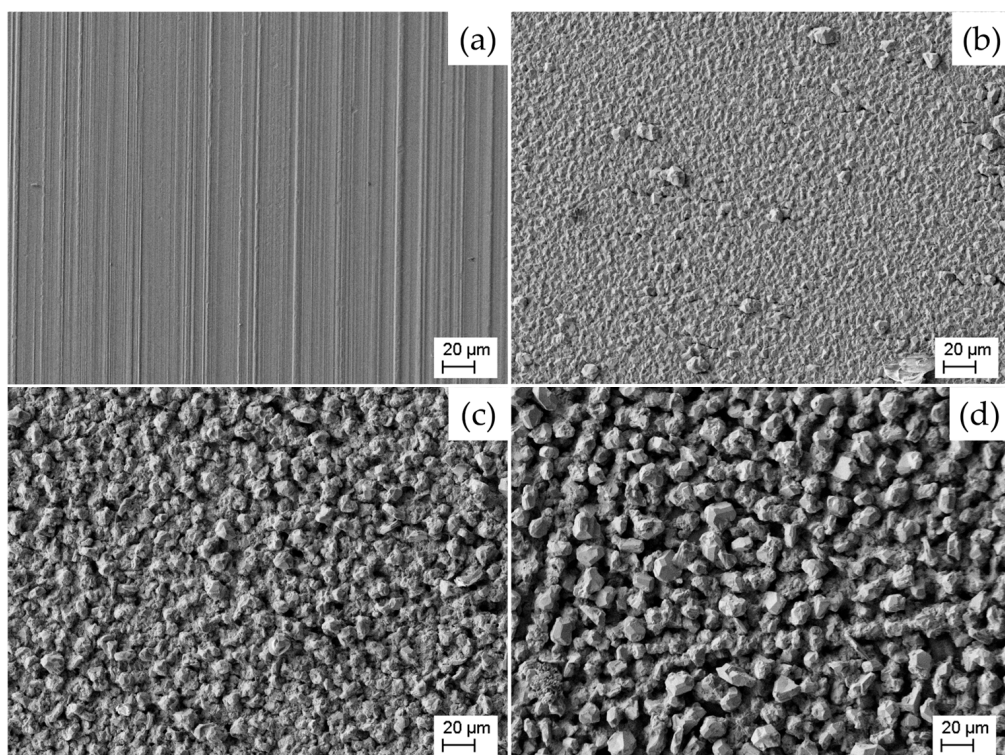


**Figure 5.** Scanning electron microscope images with magnification of 200 $\times$  of (a) a state-of-the-art laboratory aluminum current collector foil and (b–d) electroformed aluminum foils deposited with (b) 1 rpm and 20 mA/cm $^2$ , (c) 1 rpm and 10 mA/cm $^2$  and (d) 20 rpm and 10 mA/cm $^2$ .

### 3.3. Electrochemical Characterization

Figure 6 depicts cyclic voltammograms (CVs) of the 1st and 10th cycles represented by solid and dotted lines, respectively. CVs were recorded using different aluminum foils as working electrodes in a three-electrode set-up, in the voltage range between 2.7 and 5.0 V vs. Li/Li $^+$  at a scan rate of 10 mV/s. In this configuration, lithium was used as counter and reference electrode. The aluminum foils examined in the present work include a state-of-the-art laboratory aluminum current collector foil (a) as well as electroformed ones deposited with 1 rpm and 20 mA/cm $^2$  (b), 1 rpm and 10 mA/cm $^2$  (c) and 20 rpm and 10 mA/cm $^2$  (d). The anodic current densities during the 1st cycle show noticeable differences between the various foils. However, as the cycles progress up to the 10th cycle, these differences tend to diminish and the anodic current densities converge towards close values for all the foils. The similar convergence of anodic current densities during the 10th cycle indicates that the electroformed foils can likewise be suitable for lithium-ion battery applications as current collectors.

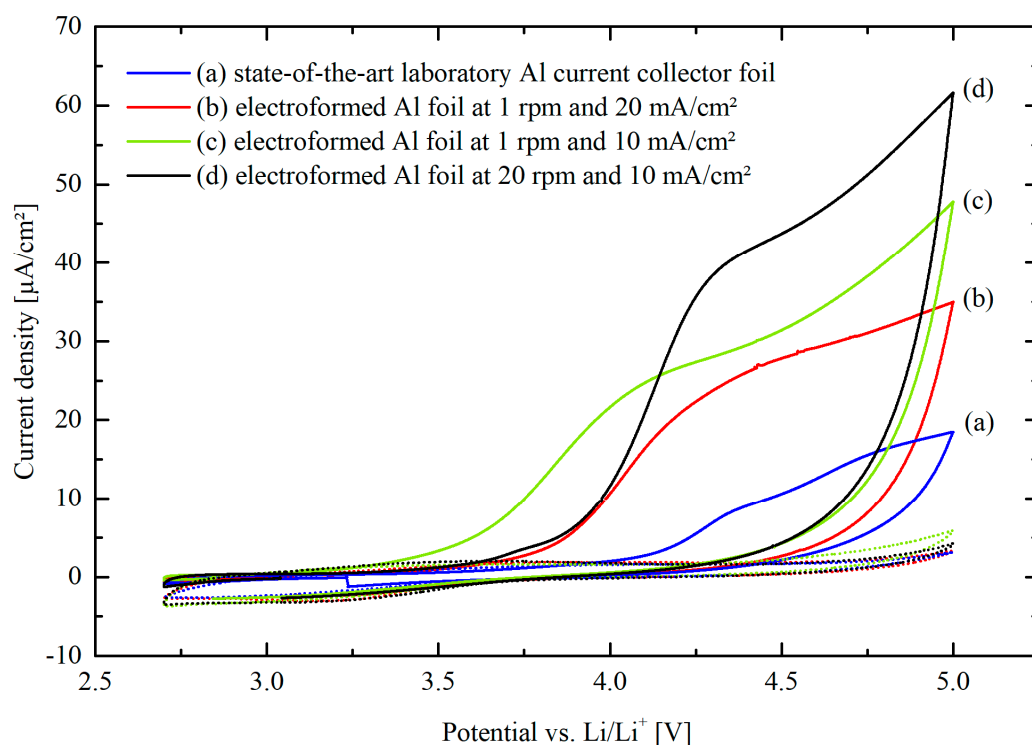


**Figure 6.** The 1st and 10th cycles (solid and dotted lines, respectively) of the CVs recorded for different aluminum foils used as working electrodes in a three-electrode set-up with lithium as counter and reference electrodes in the potential range between 2.7 and 5.0 V vs. Li/Li<sup>+</sup> at the scan rate of 10 mV/s.

#### 4. Discussion

Each of the CVs presented in Figure 6 shows an anodic peak during the 1st cycle between 4.0 and 4.4 V, followed by a subsequent increase in current densities at higher potentials. Similar results were obtained by Xia et al. [38] who recorded a CV with two cycles for scratched aluminum foil in an electrolyte consisting of 1.2 M LiPF<sub>6</sub> in EC/EMC (3:7 by volume). A scan rate of 0.1 mV/s in the potential range between 3.0 and 5.0 V vs. Li/Li<sup>+</sup> was applied. During the 2nd cycle, a strong decrease in current density was observed and assigned to the aluminum foil passivation. In a study by Myung et al. [39], a CV was recorded using a 1 M LiPF<sub>6</sub> in EC/DMC (1:1 by volume) with the same scan rate of 10 mV/s between 0 and 5.0 V vs. Li/Li<sup>+</sup>. Peaks at 3.7 and 4.7 V were recorded and attributed to the passivation reaction through the formation of AlF<sub>3</sub> on top of the naturally present Al<sub>2</sub>O<sub>3</sub> layer. Kanamura et al. [40] analyzed the passivation layer formed on aluminum in a LiPF<sub>6</sub> containing propylene carbonate electrolyte by polarizing the aluminum to 5.5 V vs. Li/Li<sup>+</sup>. The investigations showed that the layer consists of Al<sub>2</sub>O<sub>3</sub> and AlF<sub>3</sub> which confirms the results of Myung et al. [39]. Further works summarized by Zhang et al. [41] confirm that, in LiPF<sub>6</sub> containing electrolytes, an AlF<sub>3</sub> passive layer forms accompanied by the oxidation of the electrolyte. Streipert et al. [42] showed, after a long-term cycling test in 1 M LiPF<sub>6</sub> in EC/EMC (1:1 by volume) by X-ray photoelectron spectroscopy, that the main components of the passive layer are Al<sub>2</sub>O<sub>3</sub> and AlF<sub>3</sub> in addition to minor contents of further compounds. Since the current density drops sharply with increasing the cycle number, the assumption of passivation remains plausible and confirms the observation made by Xia et al. [38]. In contrast to the study of Myung et al. [39], in the present work no second anodic peak was observed. Nevertheless, the further increase in current density at higher potentials in the 1st cycle is in good agreement with the results of Xia et al. [38] and Egashira et al. [43] who demonstrated through the potential step method that the current density increases almost exponentially in the potential range of 4.5–5.5 V due to the electrolyte oxidation.

A comparison of the 1st cycle curves reveals a wide variation in anodic current densities between the different aluminum foils. This can be attributed to the different specific surface areas of the aluminum foils, in line with the cross-sectional observations shown in Figure 2 as well as the WLI images and measurements in Figure 3 and Table 2, respectively. After one cycle, the peak between 4.0 and 4.4 V disappeared and current densities at 5.0 V dropped rapidly with reaching similar values in the 10th cycle compared to the state-of-the-art laboratory aluminum current collector foil. This means that the electroformed aluminum foils passivation behavior is very satisfactory regardless of their much higher surface area and, thus, show comparable corrosion stability like the state-of-the-art laboratory aluminum current collector foil.

The specific surface area, as well as the structure of the foils, can be specifically adjusted by varying the deposition parameters, depending on the application. For example, a structured aluminum foil can be electroformed and used as a three-dimensional current collector in an LIB on which the active mass is coated. Due to the large specific surface area a higher loading by nominal area and, thus, a higher energy density on cell level can be achieved. Moreover, the three-dimensional structure enables higher charge and discharge rates to be applied, leading to higher power density. This is mainly due to a larger interface between the active mass and the current collector and, therefore, a lower charge transfer resistance compared to a flat current collector foil. Moreover, the three-dimensional structure can lead to a shortening of ion and electron pathways in the electrode and, thus, reducing of the overall resistance [44,45].

When examining the SEM images in Figure 5, it is obvious that the roughness of the electroformed aluminum foils is strongly influenced by the grain size of the deposit and the pores portion (cf. Figure 2). The decreasing of both roughness and pore portion by increasing current density and/or lowering the cylinder's rotation speed can be explained by the dependency of the electro crystallization thermodynamics and kinetics on these parameters: Higher current density and lower rotation speed lead to a more negative overpotential during aluminum deposition due to concentration polarization. With an increase in the absolute value of the overpotential, the Gibbs energy required to form a new critical nucleus decreases. With lower Gibbs Energy the nucleation rate increases according to Arrhenius' law. Consequently, deposition parameters that are leading to a more negative overpotential favor the formation of more nuclei on the surface [46–48] and lead to a denser (less porous), finer grained and smoother deposit, which can be confirmed by our results shown in Figures 2 and 5.

## 5. Conclusions

In the present work, a novel method for the manufacturing of aluminum current collectors for lithium-ion batteries was proposed. For the first time, an electroforming process from a chloride-based ionic liquid was used for this purpose. One major advantage of the electroforming process is that the current collector structure can be adjusted by choosing suitable deposition parameters. The variation of the substrate rotation speed and the current density allows to obtain dense, compact aluminum foils with low roughness and, thus, with low specific surface area. Yet, the main advantage is that the method allows for a targeted additional structure in the third dimension, allowing to obtain tailor-made highly structured foils with large specific surface area, according to the needs of the target application.

The use of structured aluminum foils holds great promise for current and future applications requiring high-power and energy density batteries. These foils offer several advantages that make them particularly interesting. Firstly, they enable higher areal active mass loading which translates into higher energy density in batteries. Secondly, the larger interface between the active mass and the current collector potentially reduces the charge transfer resistance. Finally, structured foils enable the shortening of ion and electron pathways leading to a lower electrode resistance. Both lead to a higher power density. These combined advantages make structured electroformed aluminum foils current

collectors an attractive option for applications where high power and energy densities are a key requirement.

**Author Contributions:** Conceptualization, T.S.; methodology, P.S. and M.K.; validation, P.S. and M.K.; formal analysis, P.S. and M.K.; investigation, P.S., M.K. and W.E.M.; resources, T.S.; data curation, P.S. and M.K.; writing—original draft preparation, P.S.; writing—review and editing, P.S., M.K., W.E.M. and T.S.; visualization, P.S. and M.K.; supervision, T.S.; project administration, W.E.M. and T.S.; funding acquisition, T.S. All authors have read and agreed to the published version of the manuscript.

**Funding:** This research was funded by the German Federal Ministry of Economy and Climate Protection (BMWK), grant number AiF/IGF 22140 BG/1, within the project “KultBat”. Funding from Aalen University of Applied Sciences was likewise received.

**Data Availability Statement:** Not applicable.

**Acknowledgments:** The authors appreciate the technical support of René Böttcher and the colleagues of Andreas Bund’s group at Technische Universität Ilmenau, Germany.

**Conflicts of Interest:** The authors declare no conflict of interest.

## References

1. Javed, M.S.; Zhong, D.; Ma, T.; Song, A.; Ahmed, S. Hybrid pumped hydro and battery storage for renewable energy based power supply system. *Appl. Energy* **2020**, *257*, 114026. [[CrossRef](#)]
2. Tan, K.M.; Babu, T.S.; Ramachandaramurthy, V.K.; Kasinathan, P.; Solanki, S.G.; Raveendran, S.K. Empowering smart grid: A comprehensive review of energy storage technology and application with renewable energy integration. *J. Energy Storage* **2021**, *39*, 102591. [[CrossRef](#)]
3. Fan, X.; Liu, B.; Liu, J.; Ding, J.; Han, X.; Deng, Y.; Lv, X.; Xie, Y.; Chen, B.; Hu, W.; et al. Battery Technologies for Grid-Level Large-Scale Electrical Energy Storage. *Trans. Tianjin Univ.* **2020**, *26*, 92. [[CrossRef](#)]
4. Zhang, C.; Wei, Y.-L.; Cao, P.-F.; Lin, M.-C. Energy storage system: Current studies on batteries and power condition system. *Renew. Sustain. Energy Rev.* **2018**, *82*, 3091. [[CrossRef](#)]
5. Hannan, M.A.; Wali, S.B.; Ker, P.J.; Rahman, M.A.; Mansor, M.; Ramachandaramurthy, V.K.; Muttaqi, K.M.; Mahlia, T.M.I.; Dong, Z.Y. Battery energy-storage system: A review of technologies, optimization objectives, constraints, approaches, and outstanding issues. *J. Energy Storage* **2021**, *42*, 103023. [[CrossRef](#)]
6. Masias, A.; Marcicki, J.; Paxton, W.A. Opportunities and Challenges of Lithium Ion Batteries in Automotive Applications. *ACS Energy Lett.* **2021**, *6*, 621. [[CrossRef](#)]
7. Liang, Y.; Zhao, C.-Z.; Yuan, H.; Chen, Y.; Zhang, W.; Huang, J.-Q.; Yu, D.; Liu, Y.; Titirici, M.-M.; Chueh, Y.-L.; et al. A review of rechargeable batteries for portable electronic devices. *InfoMat* **2019**, *1*, 6. [[CrossRef](#)]
8. Winter, M.; Barnett, B.; Xu, K. Before Li Ion Batteries. *Chem. Rev.* **2018**, *118*, 11433. [[CrossRef](#)]
9. Kim, T.; Song, W.; Son, D.-Y.; Ono, L.K.; Qi, Y.J. Lithium-ion batteries: Outlook on present, future, and hybridized technologies. *Mater. Chem. A* **2019**, *7*, 2942.
10. Armand, M.; Axmann, P.; Bresser, D.; Copley, M.; Edström, K.; Ekberg, C.; Guyomard, D.; Lestriez, B.; Novák, P.; Petranikova, M.; et al. Lithium-ion batteries—Current state of the art and anticipated developments. *J. Power Sources* **2020**, *479*, 228708. [[CrossRef](#)]
11. Warner, J.T. *Lithium-Ion Battery Chemistries. A Primer*, 1st ed.; Elsevier: Cambridge, MA, USA, 2019.
12. Zhang, Y.S.; Courtier, N.E.; Zhang, Z.; Liu, K.; Bailey, J.J.; Boyce, A.M.; Richardson, G.; Shearing, P.R.; Kendrick, E.; Brett, D.J.L. A Review of Lithium-Ion Battery Electrode Drying: Mechanisms and Metrology. *Adv. Energy Mater.* **2022**, *12*, 2102233. [[CrossRef](#)]
13. Warner, J.T. *The Handbook of Lithium-Ion Battery Pack Design. Chemistry, Components, Types and Terminology*, 1st ed.; Elsevier: Amsterdam, The Netherlands, 2015.
14. Zhou, S.; Liu, G.; Ding, N.; Shang, L.; Dang, R.; Zhang, J. Improved performances of lithium-ion batteries by graphite-like carbon modified current collectors. *Surf. Coat. Technol.* **2020**, *399*, 126150. [[CrossRef](#)]
15. He, L.-P.; Sun, S.-Y.; Song, X.-F.; Yu, J.-G. Recovery of cathode materials and Al from spent lithium-ion batteries by ultrasonic cleaning. *Waste Manag.* **2015**, *46*, 523. [[CrossRef](#)]
16. Lain, M.J.; Brandon, J.; Kendrick, E. Design Strategies for High Power vs. High Energy Lithium Ion Cells. *Batteries* **2019**, *5*, 64. [[CrossRef](#)]
17. Song, J.-M.; Zou, Y.-S.; Kuo, C.-C.; Lin, S.-C. Orientation dependence of the electrochemical corrosion properties of electrodeposited Cu foils. *Corros. Sci.* **2013**, *74*, 223. [[CrossRef](#)]
18. Cao, Q.-D.; Fang, L.; Lv, J.-M.; Zhang, X.-P.; Thuy Dat, N. Effects of pulse reverse electroforming parameters on the thickness uniformity of electroformed copper foil. *Trans. IMF* **2018**, *96*, 108. [[CrossRef](#)]
19. Zhu, P.; Gastol, D.; Marshall, J.; Sommerville, R.; Goodship, V.; Kendrick, E.J. A review of current collectors for lithium-ion batteries. *Power Sources* **2021**, *485*, 229321. [[CrossRef](#)]
20. Circuit Foil. Available online: <https://www.circuitfoil.com> (accessed on 19 July 2023).

21. Parkinson, R. *Nickel Plating and Electroforming: Essential Industries for Today and the Future*; Technical Series N° 10 088; Nickel Development Institute: Toronto, ON, Canada, 2001; pp. 1–25.
22. Heim, F.; Kreher, T.; Birke, K.P. The Influence of Micro-Structured Anode Current Collectors in Combination with Highly Concentrated Electrolyte on the Coulombic Efficiency of In-Situ Deposited Li-Metal Electrodes with Different Counter Electrodes. *Batteries* **2020**, *6*, 20. [[CrossRef](#)]
23. Feng, H.; Chen, Y.; Wang, Y. Electrochemical Performance of a Lithium Ion Battery with Different Nanoporous Current Collectors. *Batteries* **2019**, *5*, 21. [[CrossRef](#)]
24. Liang, Y.; Ding, W.; Yao, B.; Zheng, F.; Smirnova, A.; Gu, Z. Mediating Lithium Plating/Stripping by Constructing 3D Au@Cu Pentagonal Pyramid Array. *Batteries* **2023**, *9*, 279. [[CrossRef](#)]
25. Zhou, Z.; Chen, Q.; Wang, Y.; Hou, G.; Zhang, J.; Tang, Y. Pulsed Current Constructs 3DM Cu/ZnO Current Collector Composite Anode for Free-Dendritic Lithium Metal Batteries. *Batteries* **2023**, *9*, 188. [[CrossRef](#)]
26. Sörgel, S.; Kesten, O.; Wengel, A.; Sörgel, T. Nickel/sulfur composite electroplated nickel foams for the use as 3D cathode in lithium/sulfur batteries – A proof of concept. *Energy Storage Mater.* **2018**, *10*, 223–232. [[CrossRef](#)]
27. Arnet, R.; El Mofid, W.; Sörgel, T. Combining 3D Printing and Electrochemical Deposition for Manufacturing Tailor-Made 3D Nickel Foams with Highly Competitive Porosity and Specific Surface Area Density. *Metals* **2023**, *13*, 857. [[CrossRef](#)]
28. El Mofid, W.; Sörgel, T. Sulfur Loading as a Manufacturing Key Factor of Additive-Free Cathodes for Lithium-Sulfur Batteries Prepared by Composite Electroforming. *Energies* **2023**, *16*, 1134. [[CrossRef](#)]
29. Haynes, W.M.; Lide, D.R.; Bruno, T.J. *CRC Handbook of Chemistry and Physics*, 97th ed.; CRC Press: Boca Raton, FL, USA, 2016.
30. Tu, X.; Zhang, J.; Zhang, M.; Cai, Y.; Lang, H.; Tian, G.; Wang, Y. Influence of Operating Conditions on Deposition Rate and Smoothness of Electrolytic Aluminum Foil Using Chloroaluminate Ionic Liquids. *RSC Adv.* **2017**, *7*, 14790. [[CrossRef](#)]
31. Ui, K.; Kobayashi, S.; Sasaki, K.; Takeguchi, T.; Tsuda, T.; Ueda, M.; Nunomura, J.; Honkawa, Y.; Kojima, Y. Influence of Operating Conditions on Deposition Rate and Smoothness of Electrolytic Aluminum Foil Using Chloroaluminate Ionic Liquids. *J. Electrochem. Soc.* **2021**, *168*, 56510. [[CrossRef](#)]
32. Ui, K.; Kobayashi, S.; Takeguchi, T.; Tsuda, T.; Ueda, M.; Nunomura, J.; Honkawa, Y.; Oya, Y.; Kojima, Y. Influence of Pulse Electrolytic Conditions on Properties of Electrolytic Aluminum Foil Using Chloroaluminate Ionic Liquids. *Meet. Abstr.* **2021**, *MA2021-02*, 723. [[CrossRef](#)]
33. Ui, K.; Kobayashi, S.; Takeguchi, T.; Tsuda, T.; Ueda, M.; Nunomura, J.; Honkawa, Y.; Kojima, Y. Investigation on Operating Conditions Influencing the Aluminum Electrolysis Using Chloroaluminate Ionic Liquids. *Meet. Abstr.* **2020**, *MA2020-02*, 3002. [[CrossRef](#)]
34. Ui, K.; Kobayashi, S.; Kono, M.; Takeguchi, T.; Tsuda, T.; Ueda, M.; Nunomura, J.; Honkawa, Y.; Oya, Y.; Kojima, Y. (Digital Presentation) Influence of Pulse Electrolytic Conditions on Deposition Morphology of Electrolytic Aluminum Foil Using Chloroaluminate Ionic Liquids. *ECS Trans.* **2022**, *109*, 105. [[CrossRef](#)]
35. Ui, K.; Kobayashi, S.; Mandai, T.; Takeguchi, T.; Tsuda, T.; Ueda, M.; Nunomura, J.; Honkawa, Y.; Kojima, Y. Influence of Electrolytic Condition on Surface Smoothness of Electrolytic Aluminum Foil from AlCl<sub>3</sub>-EMIC Melt. *Meet. Abstr.* **2019**, *MA2019-02*, 961. [[CrossRef](#)]
36. Ui, K.; Kobayashi, S.; Takeguchi, T.; Tsuda, T.; Ueda, M.; Nunomura, J.; Honkawa, Y.; Kojima, Y. Investigation on Operating Conditions Influencing the Aluminum Electrolysis Using Chloroaluminate Ionic Liquids. *ECS Trans.* **2020**, *98*, 223. [[CrossRef](#)]
37. Ruan, S.; Schuh, C.A. Towards electroformed nanostructured aluminum alloys with high strength and ductility. *J. Mater. Res.* **2012**, *27*, 1638. [[CrossRef](#)]
38. Xia, L.; Jiang, Y.; Pan, Y.; Li, S.; Wang, J.; He, Y.; Xia, Y.; Liu, Z.; Chen, G.Z. Lithium Bis(fluorosulfonyl)imide-Lithium Hexafluorophosphate Binary-Salt Electrolytes for Lithium-Ion Batteries: Aluminum Corrosion Behaviors and Electrochemical Properties. *ChemistrySelect* **2018**, *3*, 1954. [[CrossRef](#)]
39. Myung, S.-T.; Sasaki, Y.; Sakurada, S.; Sun, Y.-K.; Yashiro, H. Electrochemical behavior of current collectors for lithium batteries in non-aqueous alkyl carbonate solution and surface analysis by ToF-SIMS. *Electrochim. Acta* **2009**, *55*, 288. [[CrossRef](#)]
40. Kanamura, K.; Okagawa, T.; Takehara, Z. Electrochemical oxidation of propylene carbonate (containing various salts) on aluminum electrodes. *J. Power Sources* **1995**, *57*, 119. [[CrossRef](#)]
41. Zhang, X.; Devine, T.M. Identity of Passive Film Formed on Aluminum in Li-Ion Battery Electrolytes with LiPF<sub>6</sub>. *J. Electrochem. Soc.* **2006**, *153*, B344. [[CrossRef](#)]
42. Streipert, B.; Röser, S.; Kasnatscheew, J.; Janßen, P.; Cao, X.; Wagner, R.; Cekic-Laskovic, I.; Winter, M.J. Influence of LiPF<sub>6</sub> on the Aluminum Current Collector Dissolution in High Voltage Lithium Ion Batteries after Long-Term Charge/Discharge Experiments. *Electrochim. Soc.* **2017**, *164*, 1474. [[CrossRef](#)]
43. Egashira, M.; Takahashi, H.; Okada, S.; Yamaki, J.-I. Measurement of the electrochemical oxidation of organic electrolytes used in lithium batteries by microelectrode. *J. Power Sources* **2001**, *92*, 267. [[CrossRef](#)]
44. Fritsch, M.; Standke, G.; Heubner, C.; Langklotz, U.; Michaelis, A.J. 3D-cathode design with foam-like aluminum current collector for high energy density lithium-ion batteries. *Energy Storage* **2018**, *16*, 125. [[CrossRef](#)]
45. Yamada, M.; Watanabe, T.; Gunji, T.; Wu, J.; Matsumoto, F. Review of the Design of Current Collectors for Improving the Battery Performance in Lithium-Ion and Post-Lithium-Ion Batteries. *Electrochim* **2020**, *1*, 124–159. [[CrossRef](#)]
46. Plieth, W. *Der Galvanische Prozess. Grundlagen der Metallabscheidung und Strukturbildung*, 1st ed.; Leuze Verlag: Bad Saulgau, Germany, 2018.

47. Paunovic, M.; Schlesinger, M. *Fundamentals of Electrochemical Deposition*, 1st ed.; Wiley: New York, NY, USA; Weinheim, Germany, 1998.
48. Plieth, W. *Electrochemistry for Materials Science*, 1st ed.; Elsevier: Amsterdam, The Netherlands; Boston, MA, USA, 2008.

**Disclaimer/Publisher's Note:** The statements, opinions and data contained in all publications are solely those of the individual author(s) and contributor(s) and not of MDPI and/or the editor(s). MDPI and/or the editor(s) disclaim responsibility for any injury to people or property resulting from any ideas, methods, instructions or products referred to in the content.